Approaching multichannel Kondo physics using correlated bosons: Quantum phases and how to realize them

Siddhartha Lal, Sarang Gopalakrishnan, and Paul M. Goldbart
Department of Physics and Institute for Condensed Matter Theory, University of Illinois at Urbana–Champaign, Urbana, Illinois 61801, USA

(Received 11 May 2010; published 16 June 2010)

We discuss how multichannel Kondo physics can arise in the setting of a localized level coupled to several bosonic Tomonaga-Luttinger liquid leads. We propose one physical realization involving ultracold bosonic atoms coupled to an atomic quantum dot, and a second, based on superconducting nanowires coupled to a Cooper-pair box. The corresponding zero-temperature phase diagram is determined via an interplay between Kondo-type phenomena arising from the dot and the consequences of direct interlead hopping, which can destabilize the Kondo ground state, thus suppressing the Kondo effect. We demonstrate that the multichannel Kondo state is stable over a wide range of parameters. We establish the existence of two nontrivial phase transitions, involving a competition between Kondo screening at the dot and strong correlations either within or between the leads (which, respectively, promote local number and phase pinning). These transitions coalesce at a self-dual multicritical point.

DOI: 10.1103/PhysRevB.81.245314 PACS number(s): 72.15.Qm, 67.85.Hj, 71.10.Pm

I. INTRODUCTION

Magnetic impurities can drastically alter the low-temperature properties of metals, leading to anomalous temperature dependence in, e.g., the heat capacity, resistance, and magnetoresistance. These properties, collectively known as the Kondo effect,[1] are exhibited when the impurity interacts antiferromagnetically with the conduction electrons of the metal and are due to the dynamic screening, as $T \to 0$, of the spins of the individual impurities by a cloud of conduction electrons. The low-energy scattering properties of each screened impurity are those of a bound but spin-polarizable impurity-cloud *singlet*, whose effects on the electron gas can be described using Fermi-liquid theory.[2] For a ferromagnetic impurity-cloud interaction, on the other hand, the spins of the impurity and its polarization cloud align; thus the system possesses two degenerate *triplet* ground states. A quantum phase transition separates the ferromagnetic and antiferromagnetic (i.e., Kondo) cases.

A striking extension of this "one-channel" Kondo effect is the multichannel version[3,4] in which each impurity couples *separately* to conduction electrons that propagate in $N(>1)$ channels (e.g., distinguished by orbital angular momentum). When $N>2s$ (with s being the spin of the impurity), the conduction electrons *overscreen* the impurity, and the low-energy behavior can no longer be described by Fermi-liquid theory; instead, the thermodynamic properties follow anomalous power laws governed by a quantum critical point.[5] In metallic systems, observing the N-channel Kondo effect has proven demanding.[6] Although advances in nanoscience have enabled the exploration of Kondo physics in the more controlled setting of semiconductor-based quantum dots[7] connected to leads (which realize the channels), even here the engineering of multichannel Kondo phenomena remains a challenge. This is primarily because of the difficulty of preventing interchannel hybridization, which gives rise at low energies to a single composite channel that screens the impurity via the one-channel Kondo effect. For instance, signatures of the two-channel Kondo effect have recently been observed in a quantum-dot-based setting[8] but accomplishing this required fine tuning to prevent hybridization.

In view of these challenges, it is desirable to explore schemes for accessing the N-channel Kondo effect and its onset in a more readily controllable setting: such settings can be achieved, e.g., using leads having tunable interparticle correlations. For the one-channel Kondo effect the possibility of such control was demonstrated in Ref. 9 in the context of a quantum-dot coupled to a Tomonaga-Luttinger liquid (TLL) lead.[10] The strength of the repulsive interactions in the lead (as encoded in the TLL parameter K) was found to tune the position of the Kondo-to-ferromagnetic phase transition. Motivated in part by this result, in the present paper we explore the case of N TLL leads coupled to a quantum dot; this case is expected to exhibit rich physics arising from the possibility of not only intralead but also interlead correlations. We focus on the case of bosonic leads because for them a wide range of K values can be experimentally accessed with relative ease: e.g., ultracold bosons with short-range repulsive interactions have $K>1$,[11] whereas ones with dipolar interactions have $K<1$.[12] We suggest two concrete realization schemes: one uses ultracold atoms;[13,14] the other uses superconducting nanowires and a Cooper-pair box.[15] Systems of ultracold atoms are especially well suited to the study of multichannel Kondo physics because their interactions are highly controllable and tunable,[11] and extraneous noise can be mitigated.

Our main theoretical results concern the competition between the N-channel Kondo effect and interactions in the leads; these interactions either suppress lead-dot tunneling or generate interlead phase locking (which would have the effect of short-circuiting the dot). Our analysis yields a phase diagram containing four distinct phases (see Fig. 4, below) and exhibiting a pair of unusual phase boundaries, which meet at a self-dual multicritical point. As discussed below, an important advantage of our proposed experimental realization of the N-channel Kondo effect is that it is robust against

interlead hybridization. We discuss the conditions for observing the N-channel Kondo effect using ultracold atoms and suggest that the unusual phase boundaries may be accessed experimentally using dipolar bosons.

II. KONDO AND RESONANT-LEVEL MODELS

We consider the general anisotropic Kondo Hamiltonian $H_K = H_{\text{leads}} + H_{\text{int}}$, where $H_{\text{leads}} = \Sigma_k v_F |k| c^\dagger_{k\sigma} c_{k\sigma}$ describes a free-electron gas (or a Fermi liquid) having Fermi velocity v_F, $c_{k\sigma}$ annihilates a conduction electron of momentum k and spin σ, and H_{int} describes the coupling to the impurity spin, which is located at $\mathbf{r}=0$,

$$H_{\text{int}} = \frac{J_\perp}{2}[S_+ c^\dagger_\downarrow(0) c_\uparrow(0) + \text{H.c.}] + \frac{J_z}{4} S_z \sum_\sigma \sigma c^\dagger_\sigma(0) c_\sigma(0),$$

where $c_\sigma(0)$ annihilates a conduction electron of spin σ at the impurity location, the Pauli matrices $\mathbf{S}$ act on the impurity spin state, and J_z and $J_\perp$, respectively, the amplitudes for the lead-dot Ising and spin-flip processes. The antiferromagnetic case, $J_z > 0$, leads to Kondo screening; at low temperatures, Kondo screening also occurs for $J_z < 0$ and $|J_\perp| > |J_z|$. However, for $J_z < 0$ and $|J_\perp| < |J_z|$, the impurity spin freezes out at low temperatures.

We shall primarily be concerned with a model that is equivalent to the Kondo model, viz., the interacting resonance-level model (iRLM). This model consists of a localized level d (i.e., a quantum dot) at the Fermi energy, hybridized with N channels of *spinless* noninteracting conduction electrons $c_{j\mathbf{k}}$, together with a short-ranged repulsion between dot and lead electrons: $H_{\text{iRLM}} = H_{\text{leads}} + H_{\text{onsite}} + H_{\text{int}}$. Here, the leads are described by $H_{\text{leads}} = \Sigma_{\mathbf{k}} \Sigma_{n=1}^N \epsilon(\mathbf{k}) c^\dagger_{n\mathbf{k}} c_{n\mathbf{k}}$ [in which $\epsilon(\mathbf{k})$ is the energy of a conduction electron of quasimomentum $\mathbf{k}$], the on-dot potential by $H_{\text{onsite}} = B d^\dagger d$, and the dot-lead couplings by

$$H^n_{\text{int}} = V[d^\dagger c_n(0) + \text{H.c.}] + U\left(d^\dagger d - \frac{1}{2}\right)\left[c^\dagger_n(0) c_n(0) - \frac{1}{2}\right], \tag{1}$$

where $V \sim J_\perp$ and $U \sim J_z + \text{const}$. The canonical transformation that maps the Kondo model on to the iRLM consists of identifying the *spin*-density waves of the Kondo model with the *particle*-density waves of the iRLM. The analogy is most evident as $U \to \infty$: the presence of an electron on the dot ensures the absence of electrons near the dot, and vice versa, i.e., an anticorrelated state resembling the Kondo singlet. The Kondo effect manifests itself in the iRLM via an enhancement, as $T \to 0$, of number fluctuations on the dot.

We now turn to the case of the iRLM with leads consisting of *interacting* electrons in one dimension, i.e., TLL leads. In this case the leads are governed by the Hamiltonian $H_{\text{leads}} = \Sigma_k E(k) b^\dagger_k b_k$ in which $\{b_k\}$ are bosonic fields that describe free collective phonon modes with linear dispersion[10] $E(k) \sim |k|$. (H_{int} is the same as in the noninteracting case discussed above.) As discussed in Ref. 9, this version of the iRLM can also be mapped on to the standard Kondo model, but the boundary between the ferromagnetic and antiferromagnetic phases depends on K, occurring at $U = \hbar v_s (\sqrt{1/2K} - 1)$, in which v_s is the speed of sound in the leads.

In the N-channel generalization of the iRLM, each channel couples independently to the impurity via H^n_{int}. By inverting the iRLM-to-Kondo mapping, one arrives at the N-channel Kondo Hamiltonian studied in Refs. 3 and 5, in which each of N channels couples independently to the spin. However, the interchannel particle transfer terms (i.e., hybridization)

$$H^{nn'}_\Gamma \sim c^\dagger_{n\alpha}(0) \sigma^i_{\alpha\beta} c_{n'\beta}(0) S^i, \tag{2}$$

which destabilize the N-channel Kondo effect, do not arise in the iRLM. This is because the particle-number (or "charge") sector of the leads in the iRLM maps on to the *spin* sector of the equivalent Kondo model. In contrast, the *particle* sector of the leads in the equivalent Kondo model has no physical significance in the iRLM and, accordingly, cannot couple to the dot. As the present work is concerned with physical realizations of the iRLM, we shall not consider terms of the form H_Γ (which are unphysical in the iRLM) further.

III. REALIZATIONS OF THE IRLM

A. Experimental setup

The first realization that we discuss involves ultracold atoms and extends the ideas of Ref. 14. A star-shaped pattern of N one-dimensional leads meeting at a point (see Fig. 1) can be constructed by passing a laser beam through a phase mask or spatial light modulator (SLM).[16] Such a device is a sheet of glass of spatially varying thickness, which distorts flat wave fronts, giving rise to a prescribed intensity pattern at a "screen" some fixed distance away. Algorithms for the construction of appropriate phase patterns are discussed in Refs. 16 and 17.

As for the dot itself, it can be realized as follows.[14] Suppose that the atoms discussed in the preceding paragraph are in a hyperfine state a. A tightly confining trap for a different hyperfine state b is now created at the intersection of the leads. An atom in state a can make a Raman transition to state b, and vice versa; while in b, it is confined at the "dot." The Raman transition thus creates a lead-dot hopping amplitude. This setup realizes an iRLM having the following couplings: K is determined by the scattering length g_{aa} for atomic state a, U by the $a \leftrightarrow b$ scattering length g_{ab}, and V by the amplitude (i.e., effective Rabi frequency) of the Raman transition. Double occupancy of the dot is prevented by a large repulsive interaction g_{bb} between atoms on the dot (provided that $g_{bb} \gg g_{aa}, g_{ab}$). All interactions are tunable via Feshbach resonances. The direct interlead hopping amplitude is governed by the intensity of the laser that traps a-state atoms at the intersection of the leads.

One can realize a similar model in a mesoscopic setting by using superconducting nanowires as the leads, together with a Cooper-pair box[15]—i.e., a superconducting island that holds at most one Cooper pair—as the dot. The normal modes of the leads are plasmon excitations, and the Hamiltonian for the box-lead system has the same form as that for the ultracold-atom system, provided the leads are connected

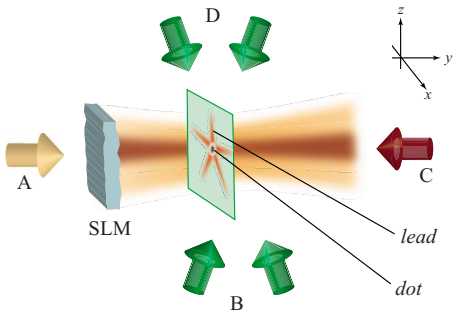

FIG. 1. (Color online) Candidate ultracold-atom setup. The spatial light modulator (SLM) distorts the wave fronts of laser A so as to create a star-shaped pattern at the "screen." Atoms are confined to the screen using two lasers (b) propagating at a relative angle $\theta \ll \pi$ so as to create an optical lattice of spacing $L = \lambda/[2\sin(\theta/2)]$. Lasers C and D are used to confine atoms in hyperfine state b at the "dot" (dark central region).

to the dot via Josephson couplings (which determine V). The coupling U is determined by the lead-dot Coulomb repulsion.

B. Interlead hopping

The geometries considered in this work, involving leads that are realized by one-dimensional tubes or wires, entail the possibility of direct interlead atomic (or electronic) hopping. One must therefore account for effects due to terms of the form $H_{\text{tunn}} \sim \tilde{t}_{nn'} c_n^\dagger(0) c_{n'}(0)$, which describe processes in which an electron hops from lead n to lead n'. We shall assume that the amplitudes $\tilde{t}_{nn'}$ are equal for all n, n': i.e., that each of the leads is connected with equal amplitude to *all* the others [see Fig. 1(c)]. In other words, we shall assume that the network of wires has the connectivity of a completely connected graph with equal hopping amplitude on each of the links. For four or five wires, such a situation can be arranged directly, by fine tuning the shape of the central barrier. A more general arrangement, which would work for an arbitrarily large number of wires, is to have a potential well for a atoms at the center of the trap that is higher in energy than all the parameters in the resonant-level model [see Fig. 1(a)]. (Note that this central island is *not* the quantum dot, which is created by the potential for b atoms.) Such a site would not appear in the effective low-energy description; instead, upon being integrated out, it would generate interlead hopping terms that would have the same value for any pair of leads. These terms could be tuned by changing the depth of the optical potential for a atoms at the center of the star shape in Fig. 2. It is important to note that we are assuming that the energy cost Δ for the occupation of the central island exceeds all other energy scales in the problem. Therefore, the lifetime of atoms on the island is approximately $\hbar/\Delta$; because this is smaller than any other time scale in the problem, the island-mediated interlead tunneling process may be treated as being instantaneous.

Relaxing the assumption of large Δ would lead to the appearance of Coulomb-blockade physics associated with the on-site cost for having multiple particles on the central island. Furthermore, the degree of freedom related to the occupation of the central island would couple directly to the resonant level for the b-type atoms (i.e., to the dot); such a coupling might generate an operator that leads away from the multichannel Kondo fixed point and toward the single-channel Kondo fixed point. We shall avoid such complications in the present work by restricting ourselves to large values of Δ.

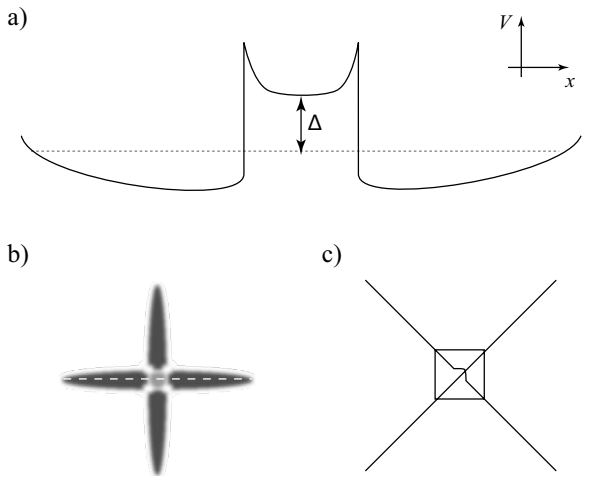

FIG. 2. (a) Schematic representation of the optical potential experienced by a-type atoms. The dotted gray line marks the chemical potential. Interlead tunneling is mediated by the central island, the occupation of which costs an energy Δ. For Δ larger than the other relevant energy scales, the central island can be integrated out to yield an *instantaneous* interlead hopping element. (b) The two-dimensional geometry in the plane to which the atoms are confined, including the central island. The shading indicates the local depth of the optical potential; darker gray implies a deeper potential. The dashed line indicates the longitudinal section sketched in panel (a). (c) Effective connectivity, at low energies, of the four wires: each wire is coupled to every other wire with equal strength, as explained in the text.

C. Accessible parameter range

For the cold-atomic case, the coupling constant U is given by the approximate expression[14,18]

$$U = \frac{\hbar^2 a_{ab}}{2m a_0^3}(n_{1D} a_0) \times f, \tag{3}$$

where a_{ab} is the (three-dimensional) scattering length between species a and b, m is the atomic mass, a_0 is the width of the harmonic-oscillator ground-state wave function in each of the tightly confined directions, n_{1D} is the number of atoms per unit length in each lead (near the center of the trap), and f is a dimensionless parameter that measures the extent of wave-function overlap between the leads and the dot. In order to realize the topology described in the previous section for $N > 3$, one must prevent nearest-neighbor tunneling between the leads; this limits f to be at most $1/N$, where N is the number of leads. (As the Kondo temperature decreases with f, this bound limits the number of channels that it is feasible to realize using the approach described here.) The other important parameters are the coupling constant V

and the speed of sound. The former is given by the expression $V=\hbar\Omega$, where Ω is the effective Rabi frequency of the Raman transition coupling the hyperfine states a and b. The speed of sound is given by the expression

$$v_s = \frac{\hbar\pi n_{1D}}{mK}, \tag{4}$$

where K is the Luttinger parameter. There is no general, closed-form expression for the Luttinger parameter in terms of the microscopic variables; however, as discussed in Sec. I and in Refs. 11 and 12, essentially the entire range of K values is experimentally accessible. As we shall show in what follows, the Kondo temperature depends on the microscopic parameters according to the general form

$$k_B T_K \sim \frac{\hbar v_s}{\xi}\exp\left(-\frac{\hbar v_s}{\xi U}\right), \tag{5}$$

where ξ is the healing length of the Bose gas (which is typically on the order of interparticle spacing). For ^{87}Rb atoms in a trap with transverse dimensions about 40 nm (see, e.g., Ref. 18), and for $K\approx 1$ (i.e., the Tonks-Girardeau limit), one can reasonably attain $U\approx 20$ nK, $\hbar v_s/\xi\approx 70$ nK, and hence $T_K\approx 5-10$ nK; such temperatures are routinely achieved in ultracold atomic settings. It should be possible to increase T_K further by tuning a_{ab} through a Feshbach resonance, or, alternatively, by using Na instead of Rb.

IV. ANALYSIS OF THE MODEL

In this section, we develop the phase diagram for the iRLM with TLL leads using perturbative renormalization-group (RG) techniques. In addition to processes that involve the dot, we account for those in which bosons hop directly between leads. It is useful to write the Hamiltonian for the uncoupled leads as

$$H_{\text{leads}} = \sum_{n=1}^{N}\frac{v_s}{2\pi}\int_0^L dx\left[K(\partial_x\theta_n)^2 + \frac{1}{K}(\partial_x\phi_n)^2\right], \tag{6}$$

where the density fluctuation modes of the TLLs are given by the operators $\rho_n(x)\sim\partial_x\phi_n(x)/\pi$ and the canonically conjugate momenta are given by $\partial_x\theta_i(x)$. Direct hopping processes between the leads can be described using the boson annihilation/creation operators $\psi_n(x)\sim e^{i\theta_n(x)}|_{x=0}$ at the end points of the semi-infinite TLLs,

$$H_{\text{tunn}} = t\sum_{n,n'}\{e^{i[\theta_n(0)-\theta_{n'}(0)]} + \text{H.c.}\}. \tag{7}$$

An RG analysis of this interlead hopping term about a system of N decoupled wires gives the RG flow equation for the hopping amplitude t as

$$\frac{dt}{dl} = \left(1-\frac{1}{K}\right)t. \tag{8}$$

Therefore, the fixed point characterizing a system of N decoupled wires (which we shall refer to as the disconnected fixed point, DFP, $t=0$) is stable for $K<1$. At low frequencies, the ground state of the complete system consists of either N uncorrelated wires (i.e., the DFP), or N maximally correlated wires [which we shall refer to as the connected fixed point (CFP), at which $t\to\infty$]. The CFP manifests itself via the mutual pinning of the phase fields at the junction,

$$\theta_n(x,t) = \theta_{n'}(x,t)|_{x=0} \tag{9}$$

for all pairs (n,n').[19] Additionally, current conservation at the junction demands that

$$\sum_{n=1}^{N}\partial_t\theta_n(0,t) = 0. \tag{10}$$

In the language of the RG, the hopping t flows to 0 (i.e., to the DFP) for $K<1$,[20] and to strong coupling (i.e., to the CFP) for $K>1$.[19,20] An RG analysis around the CFP reveals that the leading perturbation is given by the backscattering process on, say, the jth lead close to the junction ($x=0$) having amplitude λ,[10,20]

$$S_{back} = -\lambda\int d\tau\cos[\phi_j(x_j=0,\tau)] \tag{11}$$

in Euclidean space time. It is worth emphasizing that the form of this perturbation arises from the well-known duality of the canonically conjugate θ and ϕ fields[10] that characterize the theory of the one-dimensional TLL leads. In the present context, which involves the dynamics of a (zero-dimensional) junction of TLLs, this duality manifests itself in its boundary version,[20] which is analogous to, e.g., the duality of number and phase variables on a superconducting island.[15] The boundary effective action has an Ohmic dissipation term[21] whose friction coefficient is given by $N/2K(N-1)$: the N lead problem is equivalent to that of quantum Brownian motion in $(N-1)$ dimensions.[22] The RG equation for the amplitude λ is

$$\frac{d\lambda}{dl} = \left[1-\frac{2(N-1)K}{N}\right]\lambda. \tag{12}$$

Therefore, the CFP is stable for $K>N/[2(N-1)]$. Both the DFP and the CFP are stable for $N/[2(N-1)]<K<1$; for K in this interval there must, therefore, be a quantum phase transition at some nonzero value of the hopping amplitude t^* separating the ground states of N uncorrelated and N maximally correlated wires. This transition is thus analogous to the localization-delocalization transition exhibited by a quantum Brownian particle on an $(N-1)$-dimensional triangular lattice in the presence of Ohmic dissipation.[22] Furthermore, computing the RG equation for the backscattering coupling λ to second order in an ϵ expansion[20,22] for $\epsilon\equiv K-N/2(N-1)$ yields an unstable fixed point at $\lambda^*=\epsilon/2$. An analogous calculation for the hopping coupling t and $\tilde{\epsilon}\equiv 1-K$ yields another unstable fixed point at $t^*=\tilde{\epsilon}/2$. In this way, the duality of the problem leads to a self-dual theory at $K=\sqrt{N/2(N-1)}$. These RG results for t, λ give rise to the RG phase diagram sketched in Fig. 3(a). Although the values of K at which the transition occurs are known analytically for weak and strong coupling, as discussed above, the precise shape of the curve in the K-t plane is not known analytically.

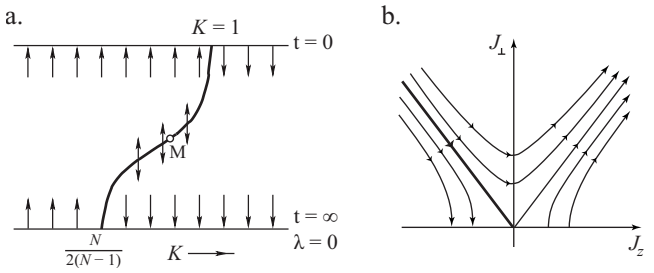

FIG. 3. (a) Phase diagram for N leads with interlead hopping t and TLL parameter K. The phase boundary (thick line) separates the disconnected (i.e., DFP, $t=0$, $K<1$) and maximally connected [i.e., CFP, $t\to\infty$, $K>N/2(N-1)$] fixed points and has a self-dual point **M** at $K=\sqrt{N/2(N-1)}$. (b) Kosterlitz-Thouless flow for lead-dot couplings at fixed (K,t). The left separatrix (thick line) demarcates the boundary between the ferromagnetic and Kondo phases.

Note that this curve of unstable fixed points at intermediate coupling turns into the marginal line at $K=1$ found previously for the case of two wires meeting at a junction.[20]

The novel feature of the N-wire phase diagram shown in Fig. 3(a) is that the CFP is stable against weak backscattering processes that take place close to the junction, even for $K<1$; this is to be contrasted with the two-wire case[20] where the CFP is unstable for all $K<1$. The enhanced stability of the CFP in the $N>2$-wire case can be understood as follows. The boundary conditions on the fields at the junction imply that a wave packet arriving at the junction from any one wire meets an effective composite TLL, comprising the $N-1$ other leads, for which $K_{\rm eff}=(N-1)K>1$. This can also be seen from the solutions of the equations of motion at the junction of the CFP, as dictated by the Griffiths current-splitting form of the boundary conditions given above.[19] The locking of the phase field in the first wire to that of the composite TLL precludes any chemical-potential drop across the junction, although only a fraction of the incoming current enters any individual lead of the composite TLL. Said another way, the local inertia of the phase fields strongly suppresses backscattering events involving high-momentum phase fluctuations. This phenomenon is dual to the enhanced inertia in the number fields at the end points of the wires at the DFP arising for $K<1$, which results in a power-law suppression of the tunneling density of states (TDOS).

We now incorporate the dot by coupling it to the N leads via $H^n_{\rm int}$ [see Eq. (1)] and develop the phase diagram via an RG analysis around the CFP and DFP. Near the CFP, we find the following scaling equations:

$$\frac{dJ_z}{dl}=J_\perp^2,\quad \frac{dJ_\perp}{dl}=\left[1-\frac{2(N-1)K}{N}+J_z\right]J_\perp, \tag{13}$$

to second order in all couplings, where the couplings have been scaled by the high-frequency cutoff $\omega_c=v_s/\xi$ (in which ξ is the healing length[14]). In addition, we find that the RG equation for the backscattering coupling acquires a contribution from the dot-mediated hopping so that

$$\frac{d\lambda}{dl}=\left[1-\frac{2(N-1)K}{N}\right]\lambda+\frac{J_\perp^2}{\omega_c}. \tag{14}$$

By shifting J_z to $J_z'\equiv J_z+1-2K(N-1)/N$, Eq. (13) assumes the well-known Kosterlitz-Thouless form[23] [see Fig. 3(b)],

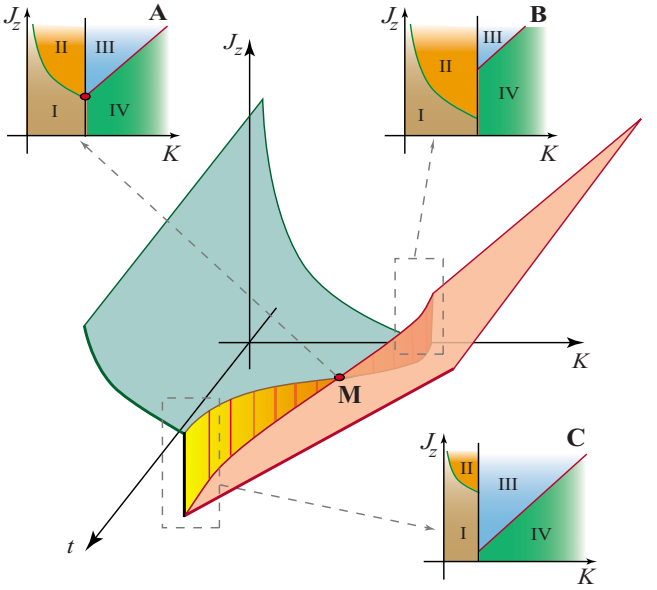

FIG. 4. (Color online) Phase diagram of the dot-lead system. The discontinuous critical surface separates the Kondo and ferromagnetic phases. The curved vertical ribbon (yellow/orange) is the phase boundary between the DFP and CFP phases [see Fig. 3(a)]. The discontinuity of the critical surface shrinks to zero at the multicritical point **M**. The diagram has four phases—I: completely decoupled wires; II: wires coupled only through dot; III: wires connected both directly and through dot; and IV: wires connected but decoupled from dot. The transitions between them (shown in insets A, B, and C) are described in the text.

with a Kondo temperature scale given by $T_K\sim\omega_c e^{-1/J_z'}$. From the discussion in Sec. III C, choosing reasonable values for $\omega_c\approx 70$ nK, $J_z'\approx 0.38-0.5$ gives a Kondo temperature of $T_K\approx 5-10$ nK. Thus, J_z is found to be RG marginal at first order but RG relevant at second order and independent of K and N. On the other hand, $J_\perp$ has the same scaling dimension as λ, and is thus dependent on K and N. For $K>[N/2(N-1)]$, even though $J_\perp$ is RG irrelevant (from its scaling dimension), it can turn relevant, due to the growth of J_z. The scaling equation for $J_\perp$ admits a nontrivial fixed point at $\tilde{J}_z\equiv[2(N-1)K/N]-1$. For $J_z>\tilde{J}_z$, all flows lead to the N-channel Kondo fixed point; for $J_z<\tilde{J}_z$, flows lead to zero dot-to-lead hopping.

If $K<[N/2(N-1)]$, the RG analysis about the CFP is invalid; one must instead analyze the Kondo couplings around the DFP. The scaling relations near the DFP are

$$\frac{dJ_z}{dl}=J_\perp^2,\quad \frac{dJ_\perp}{dl}=\left(1-\frac{1}{K}+J_z\right)J_\perp. \tag{15}$$

As with λ, the flow for t acquires a positive contribution of order $J_\perp^2/\omega_c$ from the dot-mediated hopping so that

$$\frac{dt}{dl}=\left(1-\frac{1}{K}\right)t+\frac{J_\perp^2}{\omega_c}, \tag{16}$$

i.e., the dot promotes interlead hopping, as one might expect on physical grounds. By shifting J_z to $J_z'=J_z+1-(1/K)$, Eq.

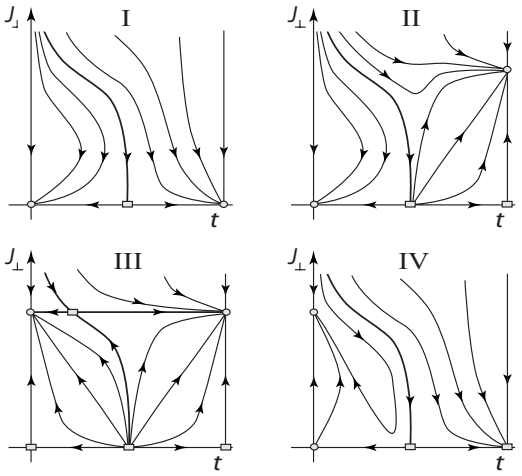

FIG. 5. RG flows in the t-$J_\perp$ plane. Here, $J_\perp \ll |J_z - J_z^*|, |J_z - \tilde{J}_z|$. (I) $J_z < J_z^*, \tilde{J}_z$: hopping via the dot is irrelevant and the dot stays disconnected. (II) $\tilde{J}_z < J_z < J_z^*$, $N/2(N-1) < K < \sqrt{N/2(N-1)}$: for $J_\perp \to 0$, hopping via the dot is irrelevant for $t < t^*$ and relevant otherwise. However, sufficiently large $J_\perp$ can drive t toward the regime in which both t and $J_\perp$ grow at low energies. (III) $J_z > J_z^*$: hopping via the dot is relevant on both sides. (IV) $\tilde{J}_z < J_z < J_z^*$, $\sqrt{N/2(N-1)} < K < 1$. Similar to II, except that $J_\perp$ competes with t to the *left* of the separatrix.

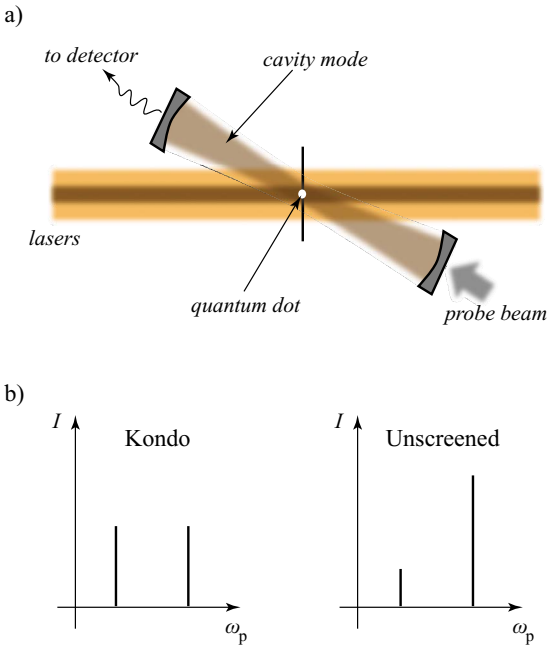

FIG. 6. (Color online) (a) Experimental setup for detecting the Kondo effect using an optical cavity. (b) Transmission through the cavity in the Kondo (left) and unscreened/ferromagnetic (right) cases. In the former case, the atomic population on the dot fluctuates coherently between 0 and 1; in the latter, the atomic population is essentially frozen at 0 or 1. The cavity's resonance frequency depends on the on-dot atomic population and can therefore be used to read out this population.

(15) assumes the Kosterlitz-Thouless form. Similarly, for $K < 1$ the scaling equation for $J_\perp$ has a nontrivial fixed point at $J_z^* = (1-K)/K$. For $J_z > J_z^*$, all flows lead to the N-channel Kondo fixed point; for $J_z < J_z^*$, flows lead to zero dot-to-lead hopping.

Bringing together the flows of $(t, J_\perp, J_z)$ yields the three-dimensional phase diagram shown in Fig. 4. The tuning of t and/or K allows one to access two nontrivial transitions between phases that have opposing characters in *both* their Kondo coupling to the dot and their direct interlead hopping. One is a transition between phase II (in which N-channel Kondo physics dominates TDOS suppression) and phase IV (in which Kondo physics is suppressed by local phase pinning); see Fig. 4(B). The other is a transition between phase I (in which Kondo physics is dominated by TDOS suppression) and phase III (in which Kondo screening overcomes local phase pinning); see Fig. 4(C). In addition, we find a multicritical point [see point **M** in Fig. 4(A)] at intermediate coupling in t; this occurs when $\tilde{J}_z = J_z^*$ [so that $K = \sqrt{N/2(N-1)}$]. Point **M** coincides with the self-dual point[22] in the phase boundary of intermediate-coupling fixed points [see Fig. 3(a)] and involves a compromise between the competing tendencies of TDOS suppression and local phase pinning. For the special case of $N=2$, the phase boundary in Fig. 4(A) becomes a marginal line at $K=1$ (i.e., the Tonks-Girardeau gas[13]), and the point **M** becomes a multicritical line at $\tilde{J}_z = J_z^* = 0$. We stress that in Fig. 4, all phase boundaries, other than the one separating the CFP and DFP, are known quantitatively. Note that this discussion is strictly valid only for small bare (i.e., microscopic) values of the lead-dot hopping amplitude $J_\perp$. For larger bare values of $J_\perp$, one must also take into account the effects of $J_\perp$ on the couplings t and λ [see Eqs.(14) and (16)]. The effects give rise to a curved phase boundary in the t-$J_\perp$ RG phase diagrams shown in Fig. 5.

The four phases are characterized by the following bare two-lead transmission coefficients across the junction: $G_2 = 0$ (i.e., minimal) at the DFP and $G_2 = 4K/N^2$ (i.e., maximal) at the CFP. These bare coefficients acquire power-law corrections of order $t^2 T^\nu$ (DFP) and $\lambda^2 T^\mu$ (CFP), arising from direct interlead scattering;[20] here, T represents an energy scale (e.g., temperature) that cuts off the RG flows, and (ν, μ) are exponents determined by the leading irrelevant perturbations around the corresponding fixed points. In experiments with ultracold atoms, these power-law contributions should be detectable via real-time dynamics of the leads.[19]

V. DETECTING THE KONDO EFFECT

We now briefly address the question of how the Kondo effect may be detected in an ultracold atomic setting. Number fluctuations on the dot can be accessed via some nondestructive measurement scheme such as, e.g., that suggested in Ref. 24 for the Bose-Hubbard model: in such a scheme the dot would be located in the waist of a high-finesse optical cavity that has a resonance frequency near an optical transition of the hyperfine state b (but not of a). This is shown in Fig. 6(a). A fixed-number state on the dot (i.e., the unscreened spin) would merely shift the cavity's resonance; by

contrast, a fluctuating-number state (i.e., the Kondo state) would lead to a double-peaked structure in the transmission spectrum of the cavity, having peaks corresponding to an empty dot and to an occupied dot [as shown in Fig. 6(b)].

VI. CONCLUSIONS

To conclude, we have delineated a scheme for realizing and observing the N-channel Kondo effect using tunable ultracold-atomic leads and proposed an additional scheme involving superconducting nanowires. The ultracold-atom-based realization involves N one-dimensional leads of bosonic atoms coupled to an atomic quantum dot. The composite lead-dot system realizes an iRLM, which is equivalent to the N-channel Kondo model. Using a perturbative RG analysis, we have established the phase diagram for this N-channel Kondo model with strongly interacting bosonic leads. The phase diagram exhibits four phases, separated by novel phase transitions arising from the interplay between the Kondo effect and the strong correlations in the leads, as well as a discontinuous phase boundary separating the Kondo and ferromagnetic phases. This phase boundary is related to the curve of unstable intermediate-coupling fixed points in the problem of N-tunnel-coupled bosonic TLL leads; the leads-only problem contains a self-dual fixed point, which becomes a multicritical point in the presence of the Kondo couplings (see Fig. 4). We have also sketched a method for the detection of the Kondo correlations at the atomic quantum dot.

We now end with some comments. First, we have seen that the problems of $N=2$ bosonic or fermionic TLL leads meeting at a junction have identical RG phase diagrams.[19,20] It is interesting to note that this result can be employed in applying our RG phase diagrams for the problem of N bosonic TLL leads to the case of a generalized Bose-Fermi-Kondo model[25] involving a spin-1/2 impurity Kondo-coupled to two fermionic TLL (Fermi) leads $[K_\rho<1(=1)]$ and $M=N-2$ Ohmic bosonic TLL leads (or, more generally, bosonic baths).[26]

Finally, we address the effects of weak asymmetries in the direct interlead tunneling and lead-dot hopping amplitudes. Asymmetries in the tunneling amplitudes involving, say, $M(<N)$ wires would result in a CFP configuration for $N-M$ wires; similarly, asymmetric lead-dot hopping amplitudes would result in an $(N-M)$-channel Kondo effect. It appears plausible that the careful design of the phase mask (which generates the optical potential wells and barriers that trap the atoms, as shown in Fig. 1) can help in ensuring that the bare values of the direct interlead hopping between $(N-M)\gg 1$ wires be made sufficiently symmetric: a $(N-M)$-channel Kondo fixed point will still be achieved in this case. Moreover, for the case of asymmetries which are small compared to the Kondo temperature, we expect that the onset of the multichannel Kondo effect should occur at significantly higher temperatures than those at which the asymmetries manifest themselves. Upon cooling the system down to arbitrarily low temperatures, however, the system would undergo a gradual crossover through a hierarchy of $M<N$-channel Kondo effects, and finally toward the single-channel effect. These crossover effects should, in principle, be detectable experimentally.[19]

ACKNOWLEDGMENTS

We thank E. Demler, M. Pasienski, and D. McKay for stimulating discussions. This work was supported by DOE under Grant No. DE-FG02-07ER46453 (S.L. and P.M.G.), through the Frederick Seitz Materials Research Laboratory at the University of Illinois at Urbana-Champaign, and NSF under Grants No. DMR-0605813 (S.L.) and No. DMR 09-06780 (S.G.).

[1] J. Kondo, Prog. Theor. Phys. **32**, 37 (1964).
[2] P. Nozières, J. Low Temp. Phys. **17**, 31 (1974).
[3] P. Nozières and A. Blandin, J. Phys. (Paris) **41**, 193 (1980).
[4] N. Andrei and C. Destri, Phys. Rev. Lett. **52**, 364 (1984); P. B. Wiegmann and A. M. Tsvelik, Z. Phys. B: Condens. Matter **54**, 201 (1985).
[5] I. Affleck, Nucl. Phys. B **336**, 517 (1990); I. Affleck and A. W. W. Ludwig, *ibid.* **352**, 849 (1991).
[6] D. L. Cox and A. Zawadowski, Adv. Phys. **47**, 599 (1998).
[7] D. Goldhaber-Gordon, H. Shtrikman, D. Mahalu, D. Abusch-Magder, U. Meirav, and M. A. Kastner, Nature (London) **391**, 156 (1998).
[8] R. M. Potok, I. G. Rau, H. Sktrikman, Y. Oreg, and D. Goldhaber-Gordon, Nature (London) **446**, 167 (2007).
[9] A. Furusaki and K. A. Matveev, Phys. Rev. Lett. **88**, 226404 (2002).
[10] T. Giamarchi, *Quantum Physics in One Dimension* (Oxford University Press, New York, 2004).
[11] I. Bloch, J. Dalibard, and W. Zwerger, Rev. Mod. Phys. **80**, 885 (2008).
[12] C. Kollath, J. S. Meyer, and T. Giamarchi, Phys. Rev. Lett. **100**, 130403 (2008); R. Citro, E. Orignac, S. De Palo, and M. L. Chiofalo, Phys. Rev. A **75**, 051602(R) (2007).
[13] B. Paredes, A. Widera, V. Murg, O. Mandel, S. Fölling, I. Cirac, G. V. Shlyapnikov, T. W. Hänsch, and I. Bloch, Nature (London) **429**, 277 (2004).
[14] A. Recati, P. O. Fedichev, W. Zwerger, J. von Delft, and P. Zoller, Phys. Rev. Lett. **94**, 040404 (2005).
[15] V. Bouchiat, D. Vion, P. Joyez, D. Esteve, and M. H. Devoret, Phys. Scr., T **T76**, 165 (1998).
[16] D. McGloin, G. C. Spalding, H. Melville, W. Sibbett, and K. Dholakia, Opt. Express **11**, 158 (2003).
[17] M. Pasienski and B. DeMarco, Opt. Express **16**, 2176 (2008).
[18] T. Kinoshita, T. Wenger, and D. S. Weiss, Nature (London) **440**, 900 (2006).
[19] A. Tokuno, M. Oshikawa, and E. Demler, Phys. Rev. Lett. **100**, 140402 (2008).
[20] C. L. Kane and M. P. A. Fisher, Phys. Rev. B **46**, 15233 (1992).
[21] A. J. Leggett, S. Chakravarty, A. T. Dorsey, M. P. A. Fisher, A. Garg, and W. Zwerger, Rev. Mod. Phys. **59**, 1 (1987).

[22] H. Yi and C. L. Kane, Phys. Rev. B **57**, R5579 (1998); H. Yi, *ibid.* **65**, 195101 (2002).
[23] J. M. Kosterlitz, J. Phys. C **7**, 1046 (1974).
[24] I. B. Mekhov, C. Maschler, and H. Ritsch, Nat. Phys. **3**, 319 (2007).
[25] J. L. Smith and Q. Si, Europhys. Lett. **45**, 228 (1999); A. M. Sengupta, Phys. Rev. B **61**, 4041 (2000).
[26] K. Le Hur and M.-R. Li, Phys. Rev. B **72**, 073305 (2005); M.-R. Li, K. Le Hur, and W. Hofstetter, Phys. Rev. Lett. **95**, 086406 (2005).